Tetrahedral displacive disorder in the scheelite-type oxide $RbReO_4$

Frederick P. Marlton[a], Bryce G. Mullens[a], Philip A. Chater[b], Brendan J. Kennedy[a*]

[a] *School of Chemistry, University of Sydney, F11, Sydney, NSW 2006, Australia*

[b] *Diamond Light Source, Harwell Science & Innovation Campus, Didcot, Oxfordshire OX11 0DE, UK*

* Address Correspondence to Brendan Kennedy (Brendan.Kennedy@Sydney.edu.au)

Abstract

Oxides exhibiting the scheelite-type structure are an important class of functional materials with notable applications in photocatalysis, luminescence and ionic conductivity. Like all materials, understanding their atomic structure is fundamental to engineering their physical properties. This study outlines a detailed structural investigation of scheelite-type oxide $RbReO_4$, which exhibits a rare long-range phase transition from $I4_1/a$ to $I4_1/amd$ upon heating. Additionally, in the long-range $I4_1/a$ model, the Re-O tetrahedral distance undergoes significant contraction upon warming. Recent studies of other scheelite oxides have attributed this apparent contraction to incoherent local scale tetrahedral rotations. In this study we use X-ray pair distribution function analysis to show that $RbReO_4$ undergoes a unique symmetry lowering process on the local scale, which involves incoherent tetrahedral displacements. The rare $I4_1/a$ to $I4_1/amd$ long-range phase transition was found to occur *via* a change from static to dynamic disorder on the local scale, which is due to the combination of the size of the *A*-site cation and lattice expansion. This demonstrates how careful manipulation of the ionic radius of the *A*-site in the scheelite structure can be used to induce local scale disorder, which has valuable implications for tailoring the physical properties of related materials.

Introduction

Scheelite-structured oxides have been identified as versatile functional materials due to their diverse range of physical and electronic properties, such as photocatalysis, luminescence, unusual magnetism and ferroelasticity[1-4]. The scheelite structure has been identified as a means to develop electronically-insulating solid electrolytes with competitive ionic conductivity for use in solid-oxide fuel cells (SOFCs)[5-6]. Scheelites have also found application in nuclear waste management[7-8].

The scheelites are a family of compounds with the chemical formula ABO_4. This structure type, containing networks of AO_8 dodecahedra and BO_4 tetrahedra, is adopted for a large variety of atomic radii and charge combinations of cations[9-10]. The archetype scheelite structure (SG $I4_1/a$, #88) features a tetragonal unit cell (Figure 1a and FigureS1-3), with the *A*- and *B*-site cations occupying special Wyckoff sites 4*a* (0, 1/4, 1/8) and 4*b* (0, 1/4, 5/8) respectively, while the oxygen anions occupy the general 16*f* (*x*, *y*, *z*) site. The AO_8 dodecahedra are described by two distinct *A*-O distances, whereas the BO_4 tetrahedra are described by a single *B*-O distance. The BO_4 tetrahedra are isolated from each other and connected to AO_8 dodecahedra *via* bridging oxygen anions. The corner-sharing polyhedra form *A*-O-*B* bridges that act as 'hinges', allowing the BO_4 tetrahedra rotational freedom.

Although the archetypical scheelite structure adopts space group $I4_1/a$, alternative symmetries have been observed by varying the ionic radius (IR) of the *A*-site cation. For example, both $CsReO_4$ and $CsTcO_4$ exhibit an orthorhombic structure with space group *Pnma* at room temperature. This structure is sometimes referred to as the pseudo-scheelite structure to highlight the similarities of the structural motifs, and is favoured as the size of the *A*-site cation increases[11-12]. Although $TlTcO_4$ also adopts the orthorhombic pseudo-scheelite structure at room temperature, $TlReO_4$ adopts a unique monoclinic structure with space group $P2_1/c$ at room temperature[11-13]. Bastide proposed that it was possible to predict the tendency for a given ABO_4 oxide to form the ideal scheelite structure based on the value of the ratio of r_A/r_O and r_B/r_O where $r_i$is the ionic radius of the eight coordinate *A*-type; six-coordinate B-type; and O anion respectively. Based on this $RbReO_4$ is predicted to be on the edge of the stability of the $I4_1/a$ structure, noting that Bastide did not consider the $I4_1/amd$ structure observed for $RbReO_4$ [14].

Tc is both a blessing and a curse: ^{99m}Tc is the most used diagnostic radioisotope, being employed in over half of all nuclear medicine procedures, whereas ^{99}Tc is the source of considerable activity in spent nuclear fuel. The management of ^{99}Tc is compounded by the stability of the water soluble pertechnetate TcO_4^- ion. In the absence of any stable Tc isotopes, Re is routinely used as a non-active surrogate. In our recent work, we showed that $RbMO_4$ (*M* = Re, Tc, Os) adopts a tetragonal structure described in space group $I4_1/a$ at room temperature[11-12, 15]. Furthermore, high-resolution

synchrotron X-ray powder diffraction (XRD) showed that RbMO$_4$ undergo a phase transition to tetragonal $I4_1/amd$ upon warming[11-12, 15]. The two tetragonal structures differ by their orientation of the BO$_4$ tetrahedra, as illustrated in Figure 1b and FigureS4-6. The $I4_1/a$ to $I4_1/amd$ transition involves the rotation of the BO$_4$ tetrahedra designated by the irreducible representation (*irrep.*) Γ_3^+.[12] Evidently the $I4_1/amd$ structure of RbMO$_4$ is the strict scheelite aristotype, although it is rarely observed. While a pressure-induced first order zircon ($I4_1/amd$) to scheelite ($I4_1/a$) phase transition has been observed in NdVO$_4$[16] and YVO$_4$[17], the tetragonal zircon structure[18] has a significantly smaller cell by approximately $1/\sqrt{2}$ along the a-axis.

There have been various studies on scheelite-structured compounds suggesting the presence of local scale disorder[12, 19-22]. In particular, variable temperature X-ray total scattering of AMoO$_4$ (A = Ca, Sr, Ba)[20-21] indicated the presence of rotational disorder of the MoO$_4$ tetrahedra in the $I4_1/a$ structure. This was influenced by both the IR of the A-site cation[20] and temperature (100 – 500 K)[21], where MoO$_4$ rotational disorder was thermally activated[21]. There is an early report of rotational disorder near the melting point of KReO$_4$ based on vibrational spectroscopy [23].

In this study, we employ variable temperature XRD and X-ray pair distribution function (PDF) to understand the rare $I4_1/a$ to $I4_1/amd$ phase transition in RbReO$_4$. Very different behaviour was observed between the long-range structure derived from the XRD and the local structure derived from the PDF. Additionally, the PDF analysis revealed a disordering mechanism upon warming, which, to our knowledge, is unique among metal oxide compounds. The identification of these structural features enables for the rational design of scheelite materials for functional applications.

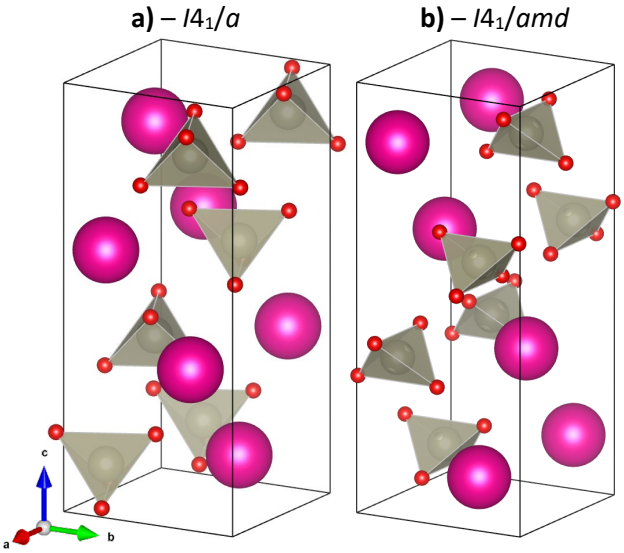

Figure 1: Representation of the scheelite structure in space group $I4_1/a$ (a) and $I4_1/amd$ (b). Additional visualizations can be viewed in FigureS1-6. The Rb, Re and O atoms are represented by fuschia, mink and red colored spheres, respectively.

Methods

The synthesis of RbReO$_4$ is outlined in our previous work[12]. X-ray total scattering experiments were performed at beamline I15-1 of the Diamond Light Source, UK (λ = 0.161669 Å, 76.69 keV). A small amount of finely ground sample was loaded into a borosilicate capillary (inner diameter of 0.78 mm) to a height of 3.5 cm. Data were collected under ambient conditions for the sample, an empty capillary, and the empty instrument. The temperature was controlled using a Cryostream (Oxford Cryosystems) for data measured in the range 100 – 500 K and a Hot Air Blower (Cyberstar) for 400 – 800 K. Both temperature devices were calibrated using an external standard prior to data collection. Diffraction data was collected using two area detectors at different distances relative to the sample for Rietveld refinement (860 mm from sample) and PDF analysis (200 mm from sample). 2D diffraction data was corrected for polarization, detector transmission and flat field, and badly performing pixels were masked, prior to integration to 1D using DAWN[24].

The PDFs G(r) were calculated using the PDFgetX3[25] software from the xPDFsuite[26] with a Q_{max} of 25 Å^{-1}. Rietveld refinements against the diffraction and PDF data were carried out using the software package TOPAS[27]. The R parameter referenced in the PDF fits is defined as follows:

$$R = \sqrt{\frac{\sum[G(r)_{obs} - G(r)_{calc}]^2}{\sum[G(r)_{obs}]^2}} \times 100$$

Where $G(r)_{obs}$ and $G(r)_{calc}$ are the observed and calculated data respectively. A broad Gaussian peak at Q ≈ 1.5 Å^{-1} was included in the Bragg Rietveld refinements to account for a feature from the capillary. A spherical correlation function was used to model the change in B_{iso} with respect to *r* in the PDF refinements[28]. Structural illustrations were drawn using the program VESTA[29].

Results

Rietveld refinements were conducted against the experimental XRD data of $RbReO_4$ using the models corresponding to the tetragonal $I4_1/a$ (100 – 790 K) and $I4_1/amd$ (400 – 790 K) structures, with example fits shown in Figure 2. The high quality fits confirm the average structure previously reported[12] and the phase purity of the sample.

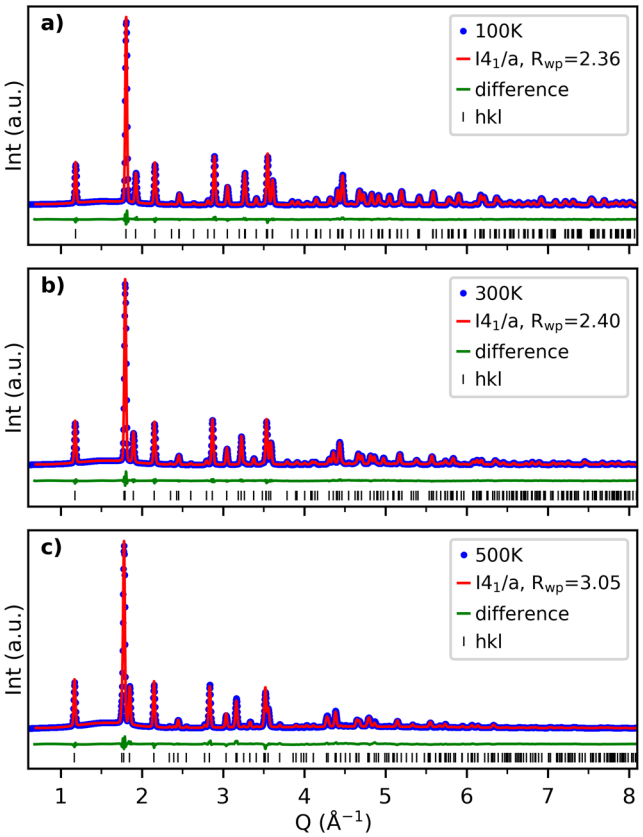

Figure 2: Fits to the X-ray Bragg data of $RbReO_4$ at 100, 300 and 500 K using the $I4_1/a$ model. The broad feature in the background around Q = 1.5 Å^{-1} is from the glass capillary used to hold the sample.

Figure 3a shows the experimental X-ray PDF of $RbReO_4$ at 100 – 500 K in increments of 100 K, with the corresponding F(Q) shown in Figure S7 and the PDF for the remaining temperatures shown in Figure S8-9. At 100 K, the local structure of $RbReO_4$ is well described by the long-range average structure of tetragonal $I4_1/a$, which is shown by the excellent small-box (aka real-space Rietveld) fit in Figure 4a. The first peak at $r \approx 1.74$ Å in Figure 3a corresponds to the Re-O distance that occurs within the ReO_4 tetrahedra. The subsequent O-O peaks are not observed due to the relatively weak scattering of oxygen with X-rays. The Rb-O peaks, which occur at $r \approx 2.8 – 3.0$ Å, along with the 2nd Re-O peak at $r \approx$ 3.5 Å, are weakly observed at 100 K. The subsequent peaks in the PDF correspond to the various cation-cation pairs in the structure, with the 5 nearest cation-cation pairs of the $I4_1/a$ model marked in Figure 3a and illustrated in Figure 3b,c. The 1st cation-cation peak ($r \approx 4.1$ Å) corresponds to a single Rb-Re distance in the *a*,*b* plane. The 2nd cation-cation peak ($r \approx 4.37$ Å) corresponds to the Re-Re, Re-Rb and Rb-Rb distances in the *a*,*c* or *b*,*c* plane, which are all equal in the $I4_1/a$ model. The 3rd cation-cation peak ($r \approx 5.82$ Å) corresponds to the equidistant Re-Re and Rb-Rb pairs along the *a*- or *b*-axis. The 4th cation-cation peak ($r \approx 6.53$ Å) corresponds to the single Re-Rb pair along the *c*-axis. The 5th cation-cation peak ($r \approx 7.27$ Å) corresponds to the next equidistant Re-Re, Re-Rb and Rb-Rb pairs involving all axes.

Observing the temperature dependence of the PDF in Figure 3 and Figure S8-9 shows that the first Re-O peak ($r \approx 1.74$ Å) appears to be unchanged, indicating the presence of rigid tetrahedra across this wide temperature range for $RbReO_4$. The remaining peaks ($r > 3.5$ Å) in the PDF data in Figure 3, which correspond to the various cation-cation pairs, show very different behavior with increasing temperature compared to the Re-O peak. The cation-cation peaks broaden with increasing temperature, which can occur due to increased thermal motion. However, observing the Rb-Rb/Re-Re peak at $r \approx 5.8$ Å, there is a significant increase in peak width at 400 and 500 K which is more indicative of splitting into multiple peak positions than simply thermal broadening of a single environment [30-31]. In the $I4_1/a$ model that describes the long-range structure at these temperatures, the Rb-Rb/Re-Re peak at $r \approx 5.8$ Å is described by a single peak, as evident in the 100 K PDF. The extra features, due to peak splitting, have been labelled with black arrows. For peak splitting to occur in the PDF, there must be multiple cation-cation distances that are not allowed by the symmetry of either the $I4_1/a$ or $I4_1/amd$ models. Similar peak splitting can be observed for $3.7 < r < 5.0$ Å, which no longer appear as a double peak at 500 K, as shown by the extra shoulder at $r \approx 4.75$ Å. This can also be observed in the full variable temperature PDF dataset in Figure S8-9. Peak splitting is indicative of differences between the local and long-range structures and suggests that symmetry lowering is occurring on the local scale of $RbReO_4$ upon warming.

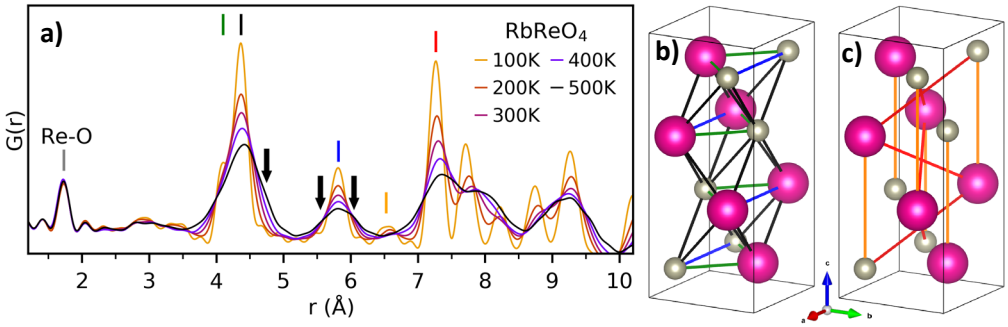

Figure 3: a) Variable temperature X-ray PDF data of $RbReO_4$ at 100, 200, 300, 400 and 500 K. Vertical markers correspond to some of the nearest atom-atom pairs in the $I4_1/a$ structure at 100 K. The color of cation-cation pairs marked in the structures in b) and c) correspond to the color of the markers in a). In b,c) the Rb, Re are represented by fuschia and mink colored spheres, respectively, while the oxygen atoms have been omitted. Black arrows in a) indicate extra features in the PDF at 400 and 500 K that are not described by the $I4_1/a$ model.

Fits to the PDF data were conducted using the long-range models of tetragonal $I4_1/a$ (100 – 790 K) and $I4_1/amd$ (550 – 790 K) for $1.2 < r < 30.0$ Å. When fitting the PDF data, a spherical correlation function was used to model the change in B_{iso} with respect to r. This accounts for the change in correlations for atom-atom pairs with shorter and longer interatomic distances[32]. Additionally, a constant B_{iso} for the O and Re sites was used for $1.2 < r < 2.3$ Å, which will be referred to as B_{local}. A single B_{local} parameter was refined against the 100 K PDF to give $B_{local} = 0.220$ (11). This was kept fixed for all temperatures and example fits (Figure 4) show that this approach did not prevent high quality fits to the PDF data, further demonstrating the rigid nature of the ReO_4 tetrahedra.

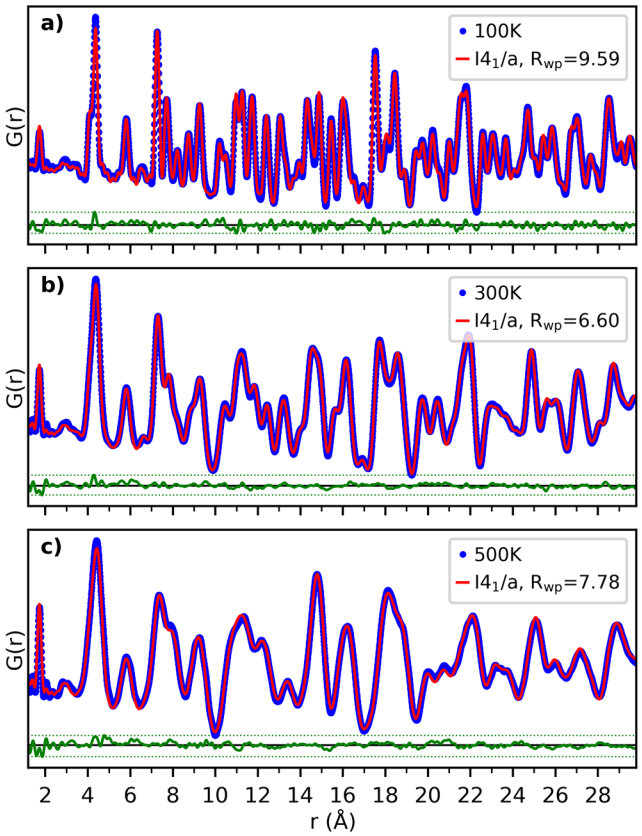

Figure 4: Fits to the X-ray PDF data of $RbReO_4$ at a) 100, b) 300 and c) 500 K using the $I4_1/a$ model.

The resultant structural parameters of interest from the fit to the PDF and diffraction data for all measured temperatures are shown in Figure 5, with a vertical black line at 615 K used to mark the $I4_1/a$ – $I4_1/amd$ phase transition. To assess the suitability of the structural models from the fits to the PDF data, R-values (Figure 5a) were calculated for $3.5 \leq r \leq 30.0$ using the equation described in the methods section. This r-range was used to assess the modelling based on the information in the PDF that significantly changes with temperature, whilst excluding the low-r termination ripples. The R_{wp}, which was output from the refinement software[27], is used to assess the quality of the Rietveld refinements against the diffraction data (Figure 5e).

In the temperature range of $100 \leq T \leq 300$ K (where T is temperature), the R-value from the PDF fitting (Figure 5a) decreases due to the broadening of the peaks, which reduces the relative intensity of the termination ripples. The R-value from the $I4_1/a$ fit at 400 K is similar to that at 300 K. This R-value remains approximately constant for $400 \leq T \leq 450$ K and then increases noticeably for $450 \leq T \leq 500$ K before becoming approximately invariant of temperature for $500 \leq T \leq 615$ K. Given there are no changes in the long-range structure between 400 and 500 K, it is unexpected for the R-value to increase with increasing temperature. These changes occur well below the phase transition temperature and will be discussed further below. After the transition to the long-range $I4_1/amd$ structure, the R-value from the PDF fitting decreases and then remains approximately constant, except for the temperatures approaching the melting point (800 K). However, the trend in the residual parameters from the modelling of the local and average structures show different behavior. This is most noticeable past the phase boundary where the long-range structure becomes $I4_1/amd$. In the Rietveld refinements, the residual parameter from the $I4_1/amd$ model is lower than the $I4_1/a$ model. However, this is the opposite in the PDF refinements. This indicates the presence of local features that the $I4_1/amd$ model cannot capture.

The lattice parameters derived from the PDF and Rietveld refinements are shown in Figure 5b,f. Throughout the measured temperature range, fits to the PDF data of $RbReO_4$ with the $I4_1/a$ model replicate the lattice parameters of the long-range structure. Equivalent lattice parameters were obtained when fitting with the $I4_1/amd$ model. The change in the trend of the lattice parameters at ~615 K corresponds to the change in the long-range structure from $I4_1/a$ to $I4_1/amd$. The phase transition switches the lattice expansion from being driven along the c-axis to the a-axis. These consistent lattice parameters between the fits to the Bragg and PDF data indicate no major distortions of the repeating unit for describing local scale correlations, despite the symmetry lowering features observed in Figure 3.

The B_{iso}, corresponding to the atomic displacement parameters (ADPs), derived from the PDF fits, is shown in Figure 5c and correspond to those describing the longer-range correlations. Observing the B_{iso} is important, because an incorrect structural model that is used to fit the PDF can result in large B_{iso} values[31]. The B_{iso} derived from the PDF refinement (Figure 5c) show very different behavior compared to those from the Rietveld refinement (Figure 5g). In the long-range structure, the Re B_{iso} is larger than the Rb B_{iso}. However, this is the opposite in the local structure. Additionally, there is a rapid increase in the Rb B_{iso} for $500 \leq T \leq 615$ K. This results in 2 different temperature dependent trends of the Rb B_{iso} for $T < 500$ K and $T > 615$ K, which is not observed in the results from the long-range modelling (Figure 5g).

The Re-O distances determined from the two types of refinements are shown in Figure 5d,h. It should be noted that the Re-O distance derived from the PDF refinement (Figure 5d) displayed significant error values (Figure S10). However, the peak position, derived from single peak fitting against the local Re-O peak in the PDF, resulted in the same trend with minimal error values. The Re-O distance shows the clearest difference between the local and long-range structural models. In the long-range structure, the Re-O distance appears to be decreasing significantly between 400 and 615 K, before becoming approximately constant for higher temperatures. Additionally, the $I4_1/amd$ model results in a shorter Re-O distance. In the local structure modelling, the Re-O distance shows very different behavior, with only subtle changes. This includes a small increase in the range 500 – 615 K. Additionally, the $I4_1/a$ and $I4_1/amd$ models result in the same Re-O distance. This is expected given that the Re-O distance derived from PDF fitting is influenced by the peak at $r \approx 1.74$ Å. This is consistent with the local *B*-O trends previously reported due to lattice expansion from chemical pressure[20], but differs from the reported trends due to thermal expansion[21].

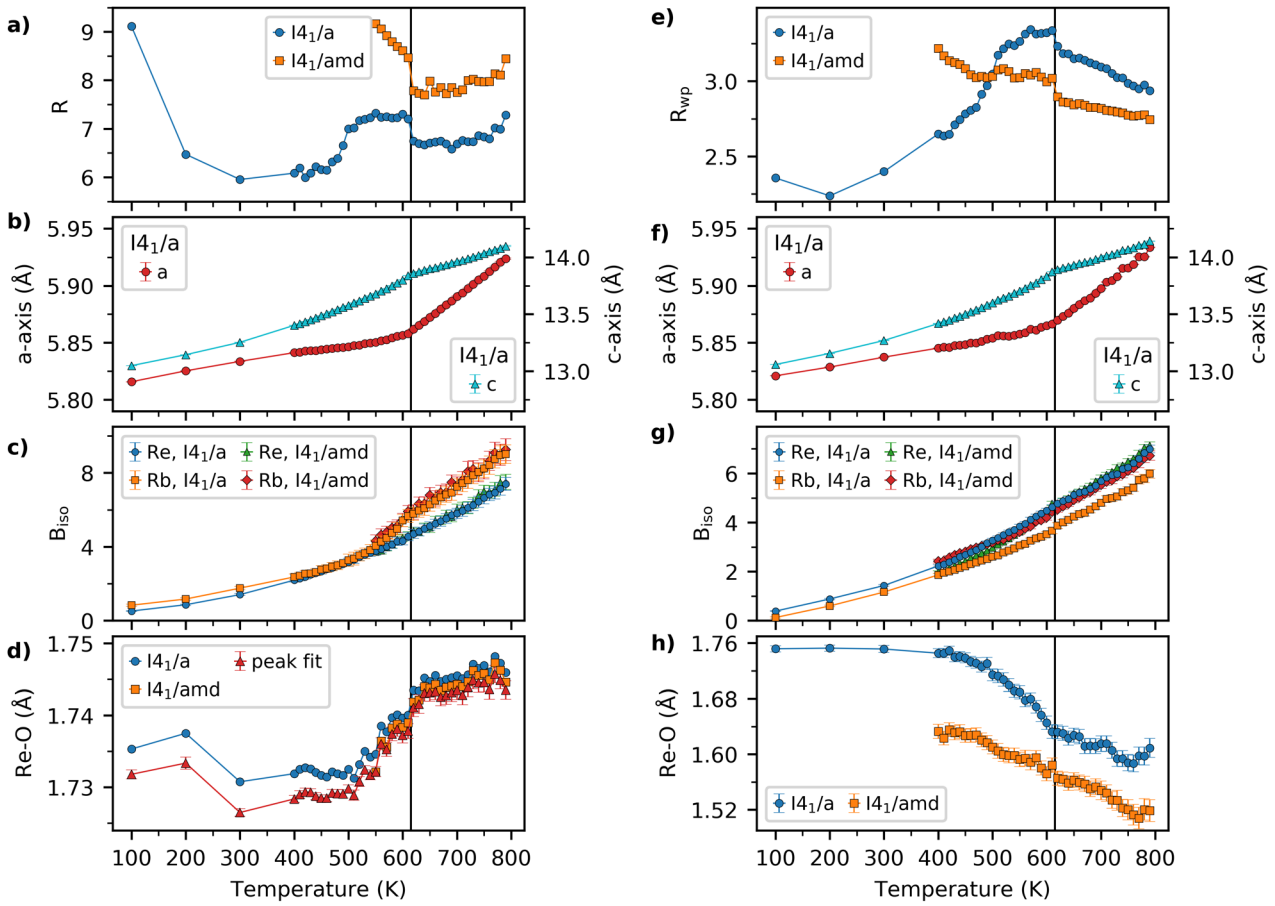

Figure 5: Results from fits of the X-ray PDF (a – d) and Bragg (e – h) data of $RbReO_4$ at 100 – 800 K using $I4_1/a$ and $I4_1/amd$ models. a,e) Residual parameters. b,f) lattice parameters from the $I4_1/a$ fits. c,g) B_{iso} of the Re and Rb sites. d,h) Re-O distances derived from fits. Vertical black line corresponds to the $I4_1/a$ to $I4_1/amd$ transition.

Discussion

Across the temperature range $100 \leq T \leq 400$ K, there are no unusual trends in the lattice parameters or B_{iso} for $RbReO_4$, although the Re-O distance shows some small variations. However, insufficient temperature points were measured in

this temperature range to draw any conclusions regarding trends. Hence, the following analysis will focus on the results from refinements for T ≥ 400 K.

Over the temperature range of 400 – 500 K, peak splitting was observed for $r > 3.5$ Å in the PDF data (Figure 3). For the same temperatures, the R-value (Figure 5a) is constant (400 – 450 K) and then increases (450 – 500 K). This unusual trend in the R-value over this temperature range is undoubtedly correlated with the peak splitting observed in the PDF data that the $I4_1/a$ structure cannot model. Over this temperature range, the Re-O distance (Figure 5d) remains constant, indicating a lack of any appreciable expansion or contraction of the ReO_4 tetrahedra. Additionally, the B_{iso} for both the Re and Rb cations from the PDF fitting (Figure 5c) gradually increase. The increase in the Re B_{iso} between 400 – 500 K indicates that upon warming, the longer-range correlations for the Re-Re and Re-Rb cation pairs are better described with a larger amount of Re atomic off-centering, *i.e.* displacement from the 4*b* (0, ¼, 5/8) site. Such off-centering of the Re cation will lift the degeneracy of the Re-O bond distances and would manifest itself in broadening of the Re-O peak. This contradicts the invariance in the Re-O peak in the PDF at $r \approx 1.74$ Å, which suggests there is no change in the Re atomic off-centering over this temperature range. This invariance is consistent with the constant B_{local} that is used to describe the Re-O peak ($1.2 < r < 2.3$ Å) in the correlation function and the approximately constant Re-O distance over 400 – 500 K. The larger B_{iso} could be a result of the split peaks, whereby the larger B_{iso} in the $I4_1/a$ model broadens the peaks of the PDF fit in the least squares minimization. This suggests the presence of incoherent tetrahedral disorder that cause deviations away from a long-range ordered structure and create split peaks in the PDF.

A possible mechanism for the peak splitting is rotation of the rigid ReO_4 tetrahedra. Thermally induced local scale tetrahedral rotations have been observed in other scheelite compounds and have been used to explain the apparent *B*-O shortening in the average structure[20-21, 33]. The way in which the structure distorts for symmetry lowering to occur is *via* rotation of the BO_4 tetrahedra[11-12], analogous to that commonly observed for the BO_6 octahedra of ABO_3 perovskites. With the lowering of symmetry, the number of possible cation-cation pairs increases due to the change in the symmetry of the unit cell[34]. For example, in the *Pnma* pseudo-scheelite unit cell[12], the different lattice parameters that describe the *a*,*b* plane results in a double peak for the cation-cation distances at $r \approx 5.8$ Å. Symmetry lowering also occurs through either ordering of different cations on the tetrahedral sites or through more complex patterns of rotation of the BO_4 tetrahedra[12, 22]. To further understand the impacts on the lattice, PDF refinements with the $I4_1/a$ model and a variable *r*-range[35] were conducted, which involved keeping $r_{min} = 1.2$ Å, but changing the value of r_{max}. This was then used to determine $\Delta l = l_2 - l_1$, where l_1 and l_2 correspond to a lattice parameter from the PDF refinement with an r_{max} of 10.0 and 30.0 Å, respectively. The resultant Δl values of interest for the $I4_1/a$ model are the *a* and *c* axes and the lattice volume (*V*), as shown in Figure 6.

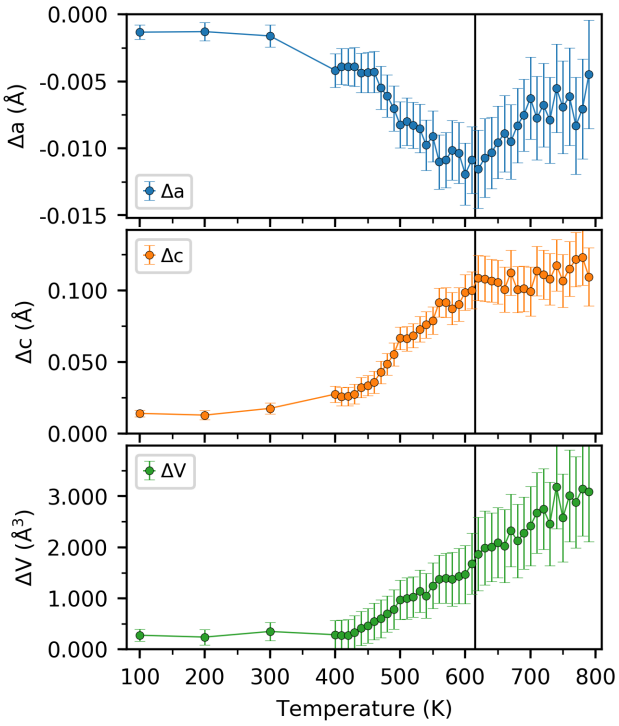

Figure 6: Results from the variable *r*-range X-ray PDF refinements with the $I4_1/a$ model. $\Delta l = l_2 - l_1$, where l_1 and l_2 correspond to a lattice parameter from the PDF refinement with an r_{max} of 10.0 and 30.0 Å, respectively. *a*, *c* and *V* correspond to the axes and volume of the tetragonal unit cell. Vertical black line corresponds to the $I4_1/a$ to $I4_1/amd$ transition.

At 100 K the Δl values are minimal, which correlates with the equivalent description of the short- and long-range structure. Similarly, no significant Δl values are observed at 200 or 300 K. For T ≥ 400 K, interesting trends in the Δl values are observed: Δa decreases slightly, while Δc and ΔV increase significantly. This suggests that for T ≥ 400 K the short-range features ($r \leq 10$ Å) are better described with a smaller lattice than the long-range average structure. This is unusual and presents further disparity between the local- and long-range structure of $RbReO_4$ for T ≥ 400 K. The local scale disordering mechanism that results in the peak splitting appears to be more exaggerated at larger length scales.

Cation displacements could be a possible mechanism for the observed peak splitting. However, this is unlikely to occur on the Re site given that the single Re-O peak at $r \approx 1.74$ Å does not split or broaden. There is the possibility of displacements of the Rb ions (*i.e.* on the *A*-site). However, if Rb displacements were the sole mechanism for the observed peak splitting upon warming, then this should not influence the temperature dependence of B_{iso} ($r > 2.3$ Å) of Re. The Re-Re correlations are impacted by the B_{iso} of Re, which increases with temperature. A further possible mechanism that would influence the Re-Re correlations is translation of the ReO_4 tetrahedra upon warming. These tetrahedral displacements are disordered such that they do not form long-range correlations, resulting in symmetry lowering of the average structure. This is consistent with the *r*-dependent trends observed in Figure 6, where at larger length scales the displacements appear more exaggerated than at smaller length scales. Although tetrahedral rotations can increase the number of cation-cation pairs, they are less likely to exhibit the same *r*-dependent trends. However, further work with neutron PDF may be necessary to confirm this. This displacive mechanism is distinct from previous temperature dependent local scale disorder mechanisms in scheelite-structured compounds[20-21, 33] and presents a new mechanism to account for the apparent decrease in the Re-O distance in the average structure (Figure 5h).

Further interesting behavior in the local structure occurs between 500 – 610 K. In particular, the significant increase in the Re-O distance and in Rb B_{iso}, that occurs before the $I4_1/a$ to $I4_1/amd$ phase transition at ~615 K. To further understand these trends, the change in the Rb B_{iso} and Re-O distance were compared to the trend from their line of best fit for 400 ≤ T ≤ 500 K. This was then used to determine $\Delta P(T) = P_{obs}(T) - P_{calc}(T)$, where P is the parameter of interest, $P_{calc}(T)$ is calculated from the curve fit for 400 ≤ T ≤ 500 K and $P_{obs}(T)$ is the observed values in Figure 5. This was also normalized by the value at $P_{obs}(650)$ to highlight the substantial changes in the Rb B_{iso} and Re-O distance for 500 ≤ T ≤ 615 K. This approach has proven highly effective in other local structure analyses[31]. The resultant curves, along with the R-value, are plotted in Figure 7 over the temperature range of 400 – 800 K.

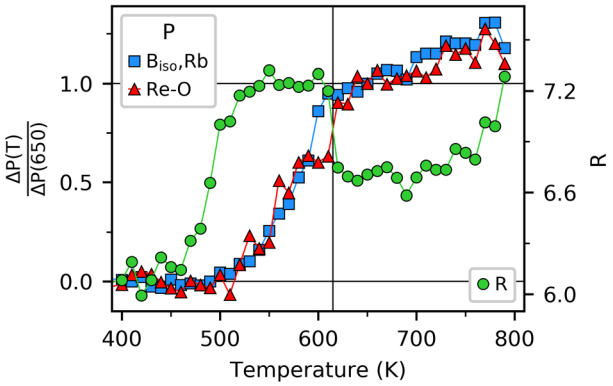

Figure 7: Normalized difference between measured and calculated parameters, P, for Rb B_{iso} and Re-O ($I4_1/a$). $\Delta P(T) = P_{obs}(T) - P_{calc}(T)$, where $P_{calc}(T)$ is determined from the line of best fit for $400 \leq T \leq 500$ K. PDF R-values have been overlaid with the right *y*-axis. Vertical black line corresponds to the $I4_1/a$ to $I4_1/amd$ transition. The horizontal black lines correspond to values of 1.0 and 0.0 for the left axis.

After increasing for $450 \leq T \leq 500$ K, the R-value stays constant for $500 \leq T \leq 610$ K, which could indicate that no further peak splitting is occurring in the PDF. However, given the increase in the B_{iso} of Re over these temperatures, it is more likely that the disordered nature of the cation-cation correlations has reached a saturation point, such that it no longer substantially changes the information present in the PDF upon warming. For $500 \leq T \leq 610$ K, the increase in the Re-O distance suggests expansion of the ReO_4 tetrahedra and the rapid increase in the Rb B_{iso} means there is a large increase in the Rb off-centering. This could indicate displacive disorder of the Rb away from the 4*a* (0, 1/4, 1/8) special position in the $I4_1/a$ model, with expansion of the rigid ReO_4 tetrahedra.

After the transition to the long-range $I4_1/amd$ structure ($T > 615$ K), the R-value from the PDF fitting decreases and then remains approximately constant, except for the temperatures approaching the melting point (800 K). A comparison between the PDF before and after the phase transition is shown in Figure S11-13, illustrating clear differences in the cation-cation peaks. The Re-O distance becomes approximately constant and the Rb B_{iso} returns to the same trend as $400 \leq T \leq 500$ K. However, deviations start to occur close to the melting temperature. The reduction in the R-value at the phase transition suggests a reduction in local scale disorder, which indicates that changes in the Rb off-centering and ReO_4 tetrahedra displacement for $500 \leq T \leq 610$ K result in more ordered cation-cation correlations. In general, high temperatures favour a high symmetry long-range structure, but with increased disorder (ADPs) of the constituent atoms. Hence, it is unlikely that increasing temperatures would result in a more ordered state of the structure. A more likely scenario is that a transition from static to dynamic disorder occurs in the temperature range $610 \leq T \leq 620$ K. This results in slightly broader features in the PDF that are more easily described by the unit cell model, resulting in a lower R-value.

There is a direct relationship between the size of the *A*-site cation, and the presence of tetrahedral rotations in scheelites. Whereas the tetragonal $I4_1/a$ structure is derived from the $I4_1/amd$ aristotype by rotation of the BO_4 tetrahedra in the *ab*-plane, the tetrahedra are rotated about the *c*-axis in the orthorhombic *Pnma* structure. In the $AReO_4$ compounds, the $I4_1/a$ to $I4_1/amd$ transition is unique for *A* = Rb[12], which has an ionic radius, IR, of 1.61 Å. For smaller *A*-site cations, such as K (IR = 1.51 Å), the structure is $I4_1/a$ and does not transition into $I4_1/amd$ upon warming[12]. For *A* = Cs (IR = 1.81 Å), the orthorhombic *Pnma* structure is observed at room temperature[12], where the tetrahedral rotations are required to satisfy the bonding requirement of the *A*-site.

In the case of $RbReO_4$, the combination of the size of Rb and thermal expansion of the unit cell gives rise to local scale distortions that deviate from the $I4_1/a$ model in order to satisfy the bonding requirement of the Rb cation. For $400 \leq T \leq 500$ K, this is in the form of tetrahedral displacements. With further lattice expansion, due to increasing temperatures ($500 \leq T \leq 610$ K), these tetrahedral distortions are no longer sufficient and expansion of the ReO_4 tetrahedra along with Rb displacements ensues. These local scale tetrahedral expansions and Rb displacements reach their limit at the phase boundary ($T \approx 615$ K), which leads to a transition from static to dynamic disordering for $T > 615$ K. There is no loss in tetrahedral displacements on the local scale, but the dynamic disorder results in the observed long-range $I4_1/amd$ symmetry. This is akin to the order-disorder model used to describe the high temperature cubic perovskite phase of $BaTiO_3$[36]. These local scale temperature dependent features in $RbReO_4$ result in the apparent unphysical trend in the Re-O distances in the long-range model (Figure 5h).

The above discussion explains why $RbMO_4$ (*M* = Re, Tc, Os) falls into the "Goldilocks zone", that allows it to exhibit the rare $I4_1/a$ to $I4_1/amd$ transition. The *A*-site cation is the perfect size to influence the bonding arrangement and distort

the tetrahedra for certain amounts of thermal expansion. With a particular threshold in temperature, the long-range $I4_1/amd$ structure, with dynamic local disorder, provides a more favourable bonding arrangement for the Rb. For *A*-site cations smaller than Rb (e.g. *A* = K), the size does not influence the bonding arrangement sufficiently to induce these tetrahedral distortions and hence the disordered $I4_1/amd$ phase does not occur. In theory it should be possible to use first principles DFT methods to establish the ground state of $RbReO_4$ and to understand the importance of the Rb cation in the valence band of this oxide. However, as decently demonstrated for $BiVO_4$ establishing an appropriate strategy to calculate the ground state of scheelite materials containing heavy cations such as Rb or Re is not trivial [37].

Conclusion

A detailed investigation of the long-range and local structure of $RbReO_4$ was conducted using variable temperature XRD and X-ray PDF. Overall, the temperature dependent structural behavior of $RbReO_4$ is much more complicated than initially anticipated. In the average structure, the $I4_1/a$ to $I4/amd$ phase transition proceeds *via* a change in the orientation of the ReO_4 tetrahedra, rotating about the *c*-axis of the unit cell[12]. Our previous work identified the nature of this phase transition by observing their modes, with the rotation of the ReO_4 tetrahedra in $I4_1/a$ designated by the *irrep* Γ_3^+.[12] However, the $I4_1/a$ average structure model also indicates significant unphysical shortening of the Re-O distances upon warming.

Analyzing the local structure showed that this is not the case, with no evidence of contraction of the ReO_4 tetrahedra with increasing temperature. It was also shown that $RbReO_4$ undergoes symmetry lowering on the local scale, evidenced by peak splitting in the PDF. This is unique from the local scale disordering observed in other scheelite oxides, where no peak splitting was reported[20-21, 33]. Previous studies have shown that symmetry lowering upon warming can occur in solid-state materials[30-31, 38], a phenomenon previously referred to as *emphanisis*. However, this was typically observed in compounds containing lone pair-bearing cations[30-31, 38]. $RbReO_4$ does not contain such cations, and hence, demonstrates unique emphanitic behaviour. These features are believed to be due to the presence of disordered ReO_4 displacements.

The rare $I4_1/a$ to $I4_1/amd$ long-range phase transition was found to occur *via* a change from static to dynamic disorder on the local scale. This is due to the combination of the size of the *A*-site cation and lattice expansion. This influences the bonding arrangement sufficiently for the locally disordered $I4_1/amd$ phase to become energetically favourable. Therefore, it is possible to induce subtle local scale distortions of the scheelite structure through careful manipulation of the IR of the cations. The importance of displacements of the Rb cations could be probed by NMR spectroscopy and the directional nature of the tetrahedral displacements probed by 3D-ΔPDF. Future investigations on the temperature dependent local structures of related compounds, such as $KReO_4$ and $CsReO_4$, should be conducted to further understand this relationship, possibly using neutron-PDF methods to increase the sensitivity to the anion sublattice. This is of great significance to the manipulation of the physical properties of scheelite structured compounds in practical applications and warrants detailed investigation of their local structure.

Acknowledgements

This work was financially supported by the Australian Research Council and was facilitated by access to Sydney Analytical, a core research facility at the University of Sydney. BGM thanks the Australian Institute for Nuclear Science and Engineering for a PGRA scholarship. Beam time at I15–1 (XPDF), Diamond Light Source is gratefully acknowledged.

Associated Content

Supporting Information Available

Additional representations of the structures $RbReO_4$. Illustration of variable temperature X-ray F(Q) data of $RbReO_4$ at 100, 200, 300, 400 and 500 K. Figures of variable temperature X-ray PDF data of $RbReO_4$ Temperature dependence of the Re-O distances derived from fits of the X-ray PDF data of RbReO4 at 100 – 800 K using $I4_1/a$ and $I4_1/amd$ models.

This information is available free of charge at the website:
https://protectau.mimecast.com/s/3sxwCoV1kpfXqkAK9U6rJBN?domain=pubs.acs.org"

References

1. Pang, L.-X.; Zhou, D.; Qi, Z.-M.; Liu, W.-G.; Yue, Z.-X.; Reaney, I. M., Structure–property relationships of low sintering temperature scheelite-structured (1 − x)$BiVO_4$–x$LaNbO_4$ microwave dielectric ceramics. *Journal of Materials Chemistry C* **2017,** *5* (10), 2695-2701.

2. Tokunaga, S.; Kato, H.; Kudo, A., Selective Preparation of Monoclinic and Tetragonal $BiVO_4$ with Scheelite Structure and Their Photocatalytic Properties. *Chemistry of Materials* **2001,** *13* (12), 4624-4628.

3. Rico, M.; Méndez-Blas, A.; Volkov, V.; Monge, M. Á.; Cascales, C.; Zaldo, C.; Kling, A.; Fernández-Díaz, M. T., Polarization and local disorder effects on the properties of Er^{3+}-doped $XBi(YO_4)_2$, X=Li or Na and Y=W or Mo, crystalline tunable laser hosts. *Journal of the Optical Society of America B* **2006,** *23* (10), 2066.

4. Singh, K.; Rajendran, M.; Devi, R.; Vaidyanathan, S., Narrow-Band Red-Emitting Phosphors with High Color Purity, Trifling Thermal and Concentration Quenching for Hybrid White LEDs and $Li_3Y_3BaSr(MoO_4)_8$:Sm^{3+}, Eu^{3+}-Based Deep-Red LEDs for Plant Growth Applications. *Inorganic Chemistry* **2022,** *61* (6), 2768-2782.

5. Cheng, J.; He, J., Electrical properties of scheelite structure ceramic electrolytes for solid oxide fuel cells. *Materials Letters* **2017,** *209*, 525-527.

6. Afif, A.; Zaini, J.; Rahman, S. M. H.; Eriksson, S.; Islam, M. A.; Azad, A. K., Scheelite type $Sr_{1-x}Ba_xWO_4$ (x = 0.1, 0.2, 0.3) for possible application in Solid Oxide Fuel Cell electrolytes. *Scientific Reports* **2019,** *9* (1), 9173.

7. Brinkman, K.; Fox, K.; Marra, J.; Reppert, J.; Crum, J.; Tang, M., Single phase melt processed powellite (Ba,Ca)MoO_4 for the immobilization of Mo-rich nuclear waste. *Journal of Alloys and Compounds* **2013,** *551*, 136-142.

8. Weaver, J.; Soderquist, C. Z.; Washton, N. M.; Lipton, A. S.; Gassman, P. L.; Lukens, W. W.; Kruger, A. A.; Wall, N. A.; McCloy, J. S., Chemical Trends in Solid Alkali Pertechnetates. *Inorganic Chemistry* **2017,** *56* (5), 2533-2544.

9. Brazdil, J. F., Scheelite: a versatile structural template for selective alkene oxidation catalysts. *Catalysis Science & Technology* **2015,** *5* (7), 3452-3458.

10. Gao, G.; Geng, Z.; Li, G.; Tan, Z.; Lu, Y.; Fan, Z.; Wang, Q.; Li, L., Understanding the Doping Chemistry of High Oxidation States in Scheelite $CaWO_4$ by Hydrothermal Conditions. *Inorganic Chemistry* **2021,** *60* (21), 16558-16569.

11. Kennedy, B. J.; Injac, S.; Thorogood, G. J.; Brand, H. E. A.; Poineau, F., Structures and Phase Transitions in Pertechnetates. *Inorganic Chemistry* **2019,** *58* (15), 10119-10128.

12. Chay, C.; Avdeev, M.; Brand, H. E. A.; Injac, S.; Whittle, T. A.; Kennedy, B. J., Crystal structures and phase transition behaviour in the 5d transition metal oxides $AReO_4$ (A = Ag, Na, K, Rb, Cs and Tl). *Dalton Transactions* **2019,** *48* (47), 17524-17532.

13. Saura-Múzquiz, M.; Marlton, F. P.; Mullens, B. G.; Manjón-Sanz, A. M.; Neuefeind, J. C.; Everett, M.; Brand, H. E. A.; Mondal, S.; Vaitheeswaran, G.; Kennedy, B. J., Understanding the Re-entrant Phase Transition in a Non-magnetic Scheelite. *Journal of the American Chemical Society* **2022**.

14. Bastide, J. P., Systématique simplifiée des composés ABX_4 (X = O2−, F−) et evolution possible de leurs structures cristallines sous pression. *Journal of Solid State Chemistry* **1987,** *71* (1), 115-120.

15. Injac, S.; Yuen, A. K. L.; Avdeev, M.; Wang, C.-H.; Turner, P.; Brand, H. E. A.; Kennedy, B. J., Structural and Magnetic Studies of ABO_4-Type Ruthenium and Osmium Oxides. *Inorganic Chemistry* **2020,** *59* (5), 2791-2802.

16. Marqueño, T.; Monteseguro, V.; Cova, F.; Errandonea, D.; Santamaria-Perez, D.; Bandiello, E.; Bettinelli, M., High-pressure phase transformations in $NdVO_4$ under hydrostatic, conditions: a structural powder x-ray diffraction study. *Journal of Physics: Condensed Matter* **2019,** *31* (23), 235401.

17. Wang, X.; Loa, I.; Syassen, K.; Hanfland, M.; Ferrand, B., Structural properties of the zircon- and scheelite-type phases of YVO_4 at high pressure. *Physical Review B* **2004,** *70* (6), 064109.

18. Hirano, M.; Morikawa, H., Hydrothermal Synthesis and Phase Stability of New Zircon- and Scheelite-Type $ZrGeO_4$. *Chemistry of Materials* **2003,** *15* (13), 2561-2566.

19. Maczka, M.; Kokanyan, E. P.; Hanuza, J., Vibrational study and lattice dynamics of disordered $NaBi(WO_4)_2$. *Journal of Raman Spectroscopy* **2005,** *36* (1), 33-38.

20. Rabuffetti, F. A.; Culver, S. P.; Suescun, L.; Brutchey, R. L., Structural Disorder in $AMoO_4$ (A = Ca, Sr, Ba) Scheelite Nanocrystals. *Inorganic Chemistry* **2014,** *53* (2), 1056-1061.

21. Culver, S. P.; Brutchey, R. L., Thermally activated rotational disorder in $CaMoO_4$ nanocrystals. *CrystEngComm* **2016,** *18* (24), 4485-4488.

22. Lacorre, P.; Pautonnier, A.; Coste, S.; Barré, M.; Béchade, E.; Suard, E., Cationic Order–Disorder in Double Scheelite Type Oxides: the Case Study of Fergusonite La_2SiMoO_8. *Inorganic Chemistry* **2021,** *60* (4), 2623-2633.

23. Gafurov, M. M.; Aliev, A. R., Changes in the local symmetry of the ReO_4^- anion near the melting point of alkali metal perrhenates. *Journal of Structural Chemistry* **2005,** *46* (5), 824-828.

24. Basham, M.; Filik, J.; Wharmby, M. T.; Chang, P. C. Y.; El Kassaby, B.; Gerring, M.; Aishima, J.; Levik, K.; Pulford, B. C. A.; Sikharulidze, I.; Sneddon, D.; Webber, M.; Dhesi, S. S.; Maccherozzi, F.; Svensson, O.; Brockhauser, S.; Náray, G.; Ashton, A. W., *Data Analysis WorkbeNch* (*DAWN*). *Journal of Synchrotron Radiation* **2015,** *22* (3), 853-858.

25. Juhas, P.; Davis, T.; Farrow, C. L.; Billinge, S. J. L., PDFgetX3: a rapid and highly automatable program for processing powder diffraction data into total scattering pair distribution functions. *Journal of Applied Crystallography* **2013,** *46* (2), 560-566.

26. Yang, X.; Juhas, P.; Farrow, C. L.; Billinge, S. J., xPDFsuite: an end-to-end software solution for high throughput pair distribution function transformation, visualization and analysis. *arXiv preprint arXiv:1402.3163* **2014**.

27. Coelho, A., TOPAS and TOPAS-Academic: an optimization program integrating computer algebra and crystallographic objects written in C++. *Journal of Applied Crystallography* **2018,** *51* (1), 210-218.

28. TOPAS User Macros. http://topas.dur.ac.uk/topaswiki/doku.php?id=macros (accessed 28/06/2022).

29. Momma, K.; Izumi, F., VESTA 3 for three-dimensional visualization of crystal, volumetric and morphology data. *Journal of Applied Crystallography* **2011,** *44* (6), 1272-1276.

30. Bozin, E. S.; Malliakas, C. D.; Souvatzis, P.; Proffen, T.; Spaldin, N. A.; Kanatzidis, M. G.; Billinge, S. J. L., Entropically Stabilized Local Dipole Formation in Lead Chalcogenides. *Science* **2010,** *330* (6011), 1660-1663.

31. Knox, K. R.; Bozin, E. S.; Malliakas, C. D.; Kanatzidis, M. G.; Billinge, S. J. L., Local off-centering symmetry breaking in the high-temperature regime of SnTe. *Physical Review B* **2014,** *89* (1), 014102.

32. Jeong, I. K.; Heffner, R. H.; Graf, M. J.; Billinge, S. J. L., Lattice dynamics and correlated atomic motion from the atomic pair distribution function. *Physical Review B* **2003,** *67* (10), 104301.

33. Amarasinghe, D. K.; Perera, S. S.; Rabuffetti, F. A., Rotational Disorder in Scheelite-Type $NaRE(MO_4)_2$ (RE = Rare-Earth, Y; M = Mo, W). *Crystal Growth & Design* **2020,** *20* (5), 3442-3448.

34. Kennedy, B. J.; Howard, C. J.; Chakoumakos, B. C., Phase transitions in perovskite at elevated temperatures - a powder neutron diffraction study. *Journal of Physics: Condensed Matter* **1999,** *11* (6), 1479-1488.

35. Culbertson, C. M.; Flak, A. T.; Yatskin, M.; Cheong, P. H. Y.; Cann, D. P.; Dolgos, M. R., Neutron Total Scattering Studies of Group II Titanates ($ATiO_3$, A^{2+} = Mg, Ca, Sr, Ba). *Scientific Reports* **2020,** *10* (1), 3729.

36. Senn, M. S.; Keen, D. A.; Lucas, T. C. A.; Hriljac, J. A.; Goodwin, A. L., Emergence of Long-Range Order in $BaTiO_3$ from Local Symmetry-Breaking Distortions. *Physical Review Letters* **2016,** *116* (20), 207602.

37. Liu, T.; Zhang, X.; Guan, J.; Catlow, C. R. A.; Walsh, A.; Sokol, A. A.; Buckeridge, J., Insight into the Fergusonite–Scheelite Phase Transition of ABO_4-Type Oxides by Density Functional Theory: A Case Study of the Subtleties of the Ground State of $BiVO_4$. *Chemistry of Materials* **2022,** *34* (12), 5334-5343.

38. Fabini, D. H.; Laurita, G.; Bechtel, J. S.; Stoumpos, C. C.; Evans, H. A.; Kontos, A. G.; Raptis, Y. S.; Falaras, P.; Van Der Ven, A.; Kanatzidis, M. G.; Seshadri, R., Dynamic Stereochemical Activity of the Sn^{2+} Lone Pair in Perovskite $CsSnBr_3$. *Journal of the American Chemical Society* **2016,** *138* (36), 11820-11832.

Table Of Content Only

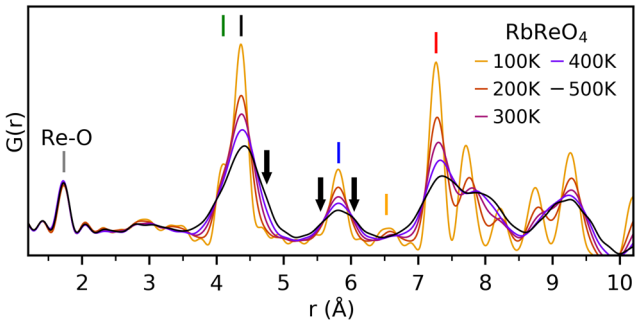

Pair distribution function analysis of X-ray total scattering data shows that the unusual $I4_1/a$ to $I4_1/amd$ phase transition in $RbReO_4$ is proceeded by local scale symmetry lowering involving incoherent tetrahedral displacements. The change from static to dynamic disorder on the local scale in this scheelite type oxides is likely to influence the average structural transition.